

Morphological instability of solid tumors in a nutrient-deficient environmentChien-Han Yen , Yi-Chieh Lai , and Kuo-An Wu **Department of Physics, National Tsing Hua University, 30013 Hsinchu, Taiwan* (Received 2 October 2022; accepted 24 April 2023; published 15 May 2023)

A phenomenological reaction-diffusion model that includes a nutrient-regulated growth rate of tumor cells is proposed to investigate the morphological instability of solid tumors during the avascular growth. We find that the surface instability could be induced more easily when tumor cells are placed in a harsher nutrient-deficient environment, while the instability is suppressed for tumor cells in a nutrient-rich environment due to the nutrient-regulated proliferation. In addition, the surface instability is shown to be influenced by the growth moving speed of tumor rims. Our analysis reveals that a larger growth movement of the tumor front results in a closer proximity of tumor cells to a nutrient-rich region, which tends to inhibit the surface instability. A nourished length that represents the proximity is defined to illustrate its close relation to the surface instability.

DOI: [10.1103/PhysRevE.107.054405](https://doi.org/10.1103/PhysRevE.107.054405)**I. INTRODUCTION**

Abnormal tumor cells have been shown, both *in vivo* and *in vitro*, to often exhibit different degrees of surface undulations during growth. The surface undulations could develop to break into surrounding tissues and potentially increase the invasiveness of tumor cells [1–3]. Therefore, the irregular surface morphology of tumors serves as a crucial prognostic factor for cancers [4,5]. Although angiogenesis has been shown to play an important role in inducing the complex morphology of solid tumors, it has been reported that the formation of irregular surfaces is also observed for tumors during avascular growth [6–9]. And antiangiogenic therapy, that reduces the nutrient and oxygen supply to the tumor cells, is shown experimentally to promote the surface instability which further causes tumor fragmentation and invasion [6,10]. This phenomenon is partly attributed to inhomogeneous spatial gradients of nutrients due to local hypoxia as a result of the treatment [6]. Nevertheless, in this paper, we show that, for avascular tumor growth, not only the morphological instability of tumors can be induced for tumors initially surrounding by a homogeneous microenvironment, but also the instability becomes stronger as the tumor is placed in a harsher environment.

To better understand the surface instability of avascular tumors, mathematical models from different perspectives, such as pressure-driven cell motion [6,7,11–22], and reaction-diffusion models [1,17–19,23–35] are developed. For instance, Greenspan [11,12] described the expansion of a tumor as a result of the internal pressure difference induced by the birth and death of cells. As the pressure gradient is large enough to overcome the surface tension of a tumor, a small undulation on the tumor surface will be enhanced. The prediction agrees with the experiment results [36]. In contrast, Chatelain *et al.* and Ben Amar *et al.* [17,18] adopted the excess Cauchy stress to characterize cell-to-cell interaction between

tumor cells. They showed analytically and numerically that a stronger repulsive Cauchy stress can trigger tumor surface instability. Also, Cristini *et al.* and Frieboes *et al.* [6,7] showed that the morphological instability would occur when the spatial gradient of the tumor velocity, which is induced by the heterogeneity of nutrient, is large enough to overcome the surface tension of spheroidal tumor surfaces, undulations on surfaces will be enhanced and subspheroids are formed. The results are consistent with experimental observations. In addition, Castro *et al.* [34] developed a chemotactically directed tumor growth reaction-diffusion model, which successfully reproduced the invasive patterns of human U87 brain tumor cells. The result of it showed that the driving force of the instability is the gradient of chemoattractant density, which drives the motion of tumor cells. As the gradient is large enough to surpass surface tension, tumor surface instability would be enhanced. Recently, cellular Potts modeling, which has been employed to study developmental biology from a cell-based perspective, has also been applied to simulate the growth, invasion, and evolution of avascular tumors [37–43]. For example, Turner and Sherratt [43] used the cellular Potts model to examine the influence of inter-cellular adhesions on the tumor invasion. They showed that tumor invasion depends not only on the cell-cell adhesion but also on the cell-medium adhesion. In addition, phase-field-like models are also developed to simulate and to investigate cancer invasion, the influence of angiogenesis, and the morphological instability of glioblastoma [44–50]. For example, Macklin *et al.* and Frieboes *et al.* [22,49] carried out phase-field-like simulations to systematically analyze the impact of the microenvironment on the morphology of solid tumors and discovered that tumor fragmentation is strongly correlated to nutrient deficiency and heterogeneity. It is clear that the morphology of the tumor is strongly influenced by the surrounding microenvironment.

In this paper, we propose a phenomenological reaction-diffusion model, that includes a nutrient-regulated growth rate for tumor cells, to describe the avascular growth of solid tumor cells. Our results indicate that the surface instability of solid tumors may be correlated to the availability of nutrients. The

*kuoan@phys.nthu.edu.tw

instability would be suppressed when tumor cells are in contact with a nutrient-rich environment. However, the instability would be more pronounced when tumor cells are placed in a harsher environment until the nutrient density is too low for tumor cells to survive. In the present model, the driving force of the instability is closely related to the diffusion of the nutrient field close to the tumor front, which is different from the instability mechanism shown in the sharp interface models that employ a constant nutrient concentration condition at the interface [11,17,18]. Furthermore, the growth moving speed of the tumor front is shown to affect the surface instability as well, but the front speed alone does not serve as a good indicator for the instability. We find that the proximity of the tumor front to the nutrient-rich region is critical to the onset of the instability, and a nourished length is defined to illustrate its close relation to the surface instability.

This paper is organized as follows: In Sec. II, a model for avascular growth of solid tumor cells is introduced, and the connection between the pressure-driven cell motion and the diffusive motion of cells employed in the present model is drawn. In Sec. III, we present a perturbative calculation on the steady moving planar front of tumor cells to examine the stability of the tumor surface. With the unperturbed front solution obtained by the shooting method, the eigenfunctions of perturbations with various wave numbers and the corresponding growth rate are readily solved using a linear stability analysis. We find that the instability is highly correlated to the availability of nutrients in the microenvironment as well as the front propagation speed. Moreover, a nourished length is defined to examine the proximity of the tumor cells to the nutrient-rich region, which is shown to be crucial to the onset of the instability.

II. MODEL FOR NUTRIENT-REGULATED AVASCULAR SOLID TUMOR GROWTH

In the early stage of solid tumor development, tumors undergo an avascular growth phase in which the growth of tumors solely depends on surrounding nutrients and there are no blood vessels involved. Given the fact that the cell proliferation is highly responsive to the availability of nutrients in the environment, the proliferation rate of solid tumors is commonly assumed to be proportional to the local nutrient density in mathematical models [6,7,12–14,16–19,34,51,52]. However, it is shown in EMT6/Ro mouse mammary tumor cells that the increase of the cell proliferation rate slows down as the nutrient density increases due to limited consumption and metabolism, and eventually the proliferation rate saturates to a constant rate [53,54]. A similar dependence is also observed for the glucose consumption rate of 9l rat brain multicell tumor spheroids [55]. Therefore, to investigate morphological instability of solid tumors subject to the nutrient-regulated growth, a set of reaction-diffusion equation describing the growth of tumors and consumption of nutrients is formulated as follows:

$$\frac{\partial n}{\partial t} = D_n \nabla^2 n + aA(u)n - \gamma n - Mn(n - \alpha)(n - \beta), \quad (1)$$

$$\frac{\partial u}{\partial t} = D_u \nabla^2 u - bnA(u), \quad (2)$$

where n and u are the tumor cell density and the nutrient density, respectively. The nutrient-regulated growth rate $aA(u)$ is approximated by a shifted hyperbolic tangent function with a growth coefficient a . The growth function $A(u)$ is

$$A(u) = \tanh\left(\frac{u - \bar{u}}{W}\right) - A_0, \quad (3)$$

where the constant A_0 is determined accordingly by requiring $A(0) = 0$ since one expects a vanishing growth rate when there is no nutrient. The constants \bar{u} and W further characterize the nutrient threshold and sensitivity for tumor growth. And γ is the apoptosis rate of tumor cells. In addition, we employ a simple cubic function $n(n - \alpha)(n - \beta)$ in the tumor cells evolution equation so that there exists two stable fixed points which correspond to a finite tumor cells state and a vanishing tumor state [56–62]. For simplicity, we set $\alpha = \beta/2$ which gives a symmetric cubic function with respect to its inflection point at α . The coefficient M is directly associated with the efforts one has to make to go from one stable fixed point to the other in nearby region. Therefore, M is closely related to the surface energy of tumor cells or the cell-cell adhesion energy. However, for nutrients, since the growth of tumor cells is proportional to the nutrient consumption, the local nutrient consumption rate is then $bnA(u)$ where b is a proportionality constant. Last, simple diffusion terms with corresponding diffusion coefficients D_n and D_u are used to describe the tumor cell movement and nutrient diffusion.

The justification of employing a diffusion description of tumor cell movement is the following. In contrast to the reaction-diffusion description of avascular tumor growth, the tumor cell movement is known to be driven by the pressure gradient of cells [6,7,12–22]. The velocity of tumor cell movement \bar{v} obeys Darcy's law $\bar{v} = -\mu \nabla P$, where μ is the mobility of tumor cells and P is the pressure of cells. Consider the solid property of tumor cells, one expects the pressure variation is related to the density variation by $dP = Kdn/n$ where K is the bulk modulus of tumor cells. Assume a homogeneous bulk modulus and mobility of tumor cells, the velocity of tumor cells can be rewritten as $\bar{v} = -(\mu K/n) \nabla n$. The local rate of change in n is the negative divergence of the cell density flux $-\nabla \cdot (n\bar{v}) = \mu K \nabla^2 n$ which justifies the above-mentioned diffusion description of cell movement. In fact, based on empirical data of human brain tumor, the product of μK ranges from 1.03×10^{-8} to 1.9×10^{-8} cm²/s [7,63–66] while the estimated diffusion coefficient is about 1.5×10^{-8} cm²/s [31]. In general, the diffusion coefficient of tumors ranges from 10^{-9} to 10^{-7} cm²/s depending on the type of tumors [31,67,68].

To further make contact with empirical data, certain parameters adopted in this work are based on reported experiments. For example, it is reported that the diffusion coefficient of brain tumors in gray matters and white matters are $D_n = 1.5 \times 10^{-8}$ cm²/s, and $D_n = 7.5 \times 10^{-8}$ cm²/s, respectively [67,68]. Take the diffusion coefficient of glucose in the cell culture medium to be $D_u = 6.7 \times 10^{-7}$ cm²/s [1,33,69,70], one obtains $D_u/D_n = 8.9$ – 44.7 . In addition, the proliferation rate and apoptosis rate of brain tumors are about 1 day⁻¹ and 0.26–0.38 day⁻¹, respectively [7,33]; the estimated consumption rate is of the order of 10^{-7} (g/cm³)/min [33]. The dimensionless forms of

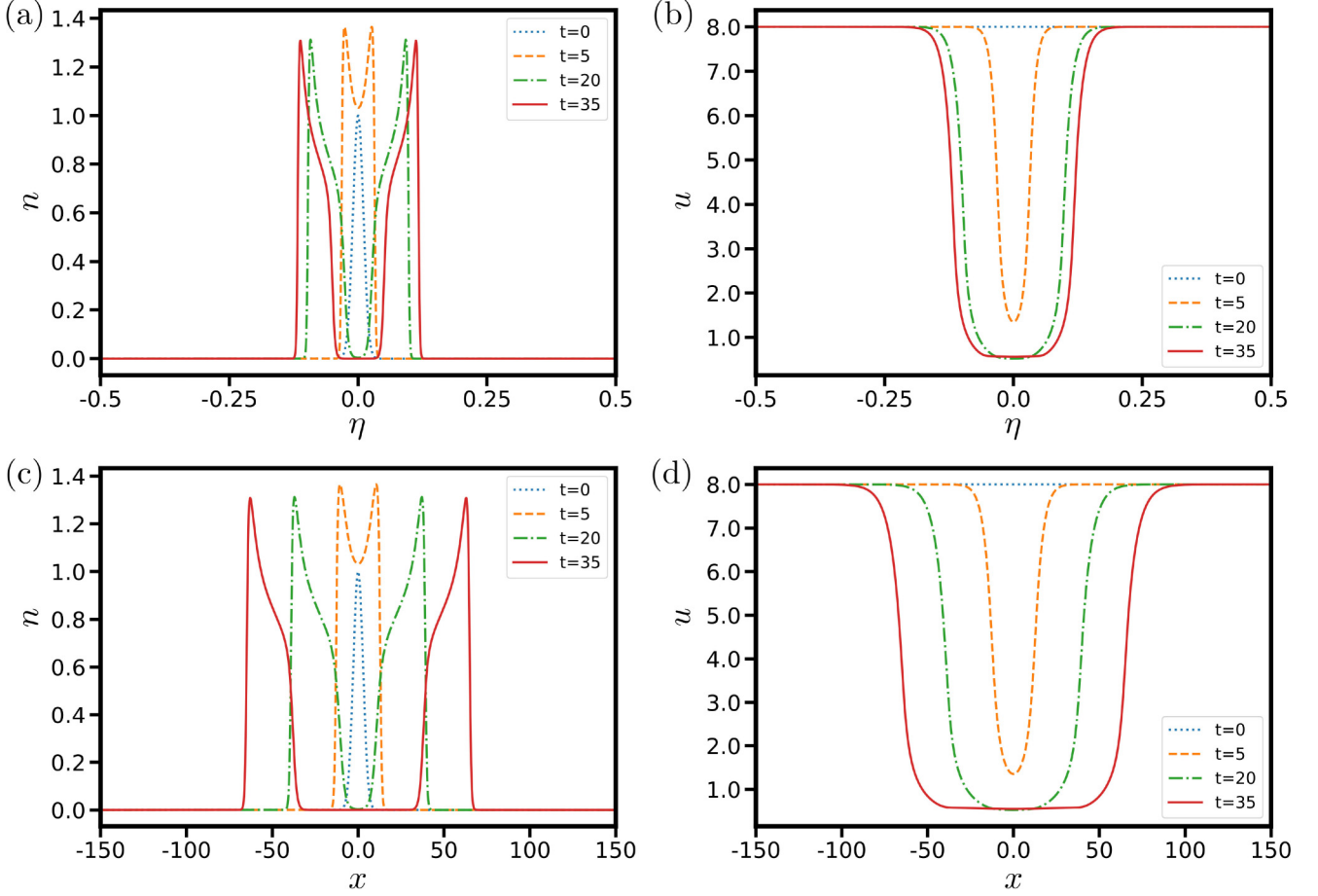


FIG. 1. Time evolution of (a) tumor cell density in η space, (b) nutrient density in η space, (c) tumor cell density in real space, and (d) nutrient density in real space. A constant nutrient density and a Gaussian shape planer tumor cell density are set initially. The simulation results are obtained with parameters $(C_0, a, \gamma, M, D_u, \bar{u}) = (8, 1, 0.4, 4.2, 10, 2)$.

Eqs. (1) and (2) are obtained by the following substitutions: $\tilde{t} = \beta b t / W$, $\tilde{\nabla} = \sqrt{D_n W} / (b\beta) \nabla$, $\tilde{u} = u / W$, $\tilde{M} = M\beta W / b$, $\tilde{a} = aW / (b\beta)$, $\tilde{\gamma} = \gamma W / (b\beta)$, $\tilde{D}_u = D_u / D_n$, $\tilde{\bar{u}} = \bar{u} / W$, $\tilde{A}_0 = -\tanh(\tilde{\bar{u}})$, $\tilde{n} = n / \beta$. Henceforth, we only handle dimensionless quantities and the tilde sign is dropped for simplicity. The dimensionless equations become

$$\frac{\partial n}{\partial t} = \nabla^2 n + anA(u) - \gamma n - Mn(n - 1/2)(n - 1), \quad (4)$$

$$\frac{\partial u}{\partial t} = D_u \nabla^2 u - nA(u), \quad (5)$$

where $A(u) = \tanh(u - \bar{u}) - A_0$. With the aforementioned empirical data, we take $D_u = 10$, $\gamma = 0.4$, $a = 1$, and M is set to be 4.2 in general.

The morphology of tumor growth is in general complex and sensitively depends on the spatial distribution of nutrients. For avascular tumor growth, the tumor consumes surrounding nutrients and grows toward the source of nutrients. As nutrients are consumed by tumor cells at the surface, less nutrients are diffused into the tumor which makes tumor cells away from the surface hard to survive and forms necrosis. Hence, to quantitatively investigate how the nutrient-regulated proliferation of cells alone affects the morphological instability of solid tumor surfaces, a planar solid tumor front in contact with

a fixed nutrient source far away from tumor cells is considered in this paper. The morphological instability of solid tumors is investigated by examining small perturbations in cell and nutrient densities perpendicular to the surface normal on the steady planar tumor front.

III. STEADY PLANAR FRONTS AND ITS STABILITY

To examine the morphological instability of planar solid tumors, the system is set up as follows. The normal of the tumor surface is chosen to be aligned in the x direction and a constant nutrient density C_0 is set up at $x = \pm\infty$, that is, $u(x = \pm\infty) = C_0$. For a planar tumor initially sits at $x = 0$, two fronts of the tumor consume nutrients and grow toward $x = +\infty$ and $x = -\infty$, respectively; see Fig. 1. Once the tumor becomes too thick, since nutrients are consumed greatly by the tumor cells near the surface, the nutrient density away from the surface becomes too low to sustain the survival of tumor cells. A necrotic region forms accordingly at the center, and steady tumor fronts moving at a constant speed are expected. The morphological instability of the tumor surface is investigated by examining small perturbations in cell and nutrient densities along the y and z directions on the planar steady tumor fronts. However, due to the rotational symmetry

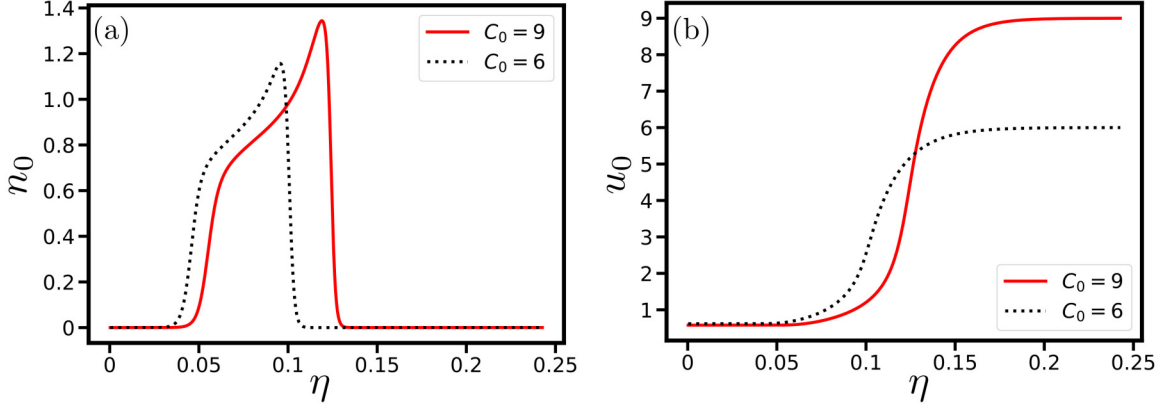


FIG. 2. Shooting solutions of (a) tumor cell density and (b) nutrient density for boundary nutrient density at $C_0 = 6$ and $C_0 = 9$, respectively. The shooting results are obtained for $(a, \gamma, M, D_u, \bar{u}) = (1, 0.4, 4.2, 10, 2)$.

around the x axis of the system, one only has to consider perturbations in one direction. Therefore, a two-dimensional system with a periodic boundary condition in the y direction and a fixed nutrient density at $\pm\infty$ in the x direction is employed in the following discussion.

A. Nontrivial solution of planar steady propagating front

To obtain the steady propagating planar front solution moving with a constant speed, one simply looks for a one-dimensional nontrivial steady propagating solution of Eqs. (4) and (5) subject to the boundary conditions: $u(x = \pm\infty) = C_0$ and $n(x = \pm\infty) = 0$. For numerical solutions and simulations, the infinite domain is handled by mapping the x space to a finite domain with the transformation, $\eta = \tanh(x/\bar{x})$, where the parameter \bar{x} is set to be 400 such that steady front profiles not far away from the origin are well resolved with a total 4096 grid points. The second derivative is transformed accordingly, we get $\partial^2/\partial x^2 = (1 - \eta^2)/\bar{x}^2 \hat{\mathcal{L}}$, where $\hat{\mathcal{L}} \equiv \partial/\partial\eta[(1 - \eta^2)\partial/\partial\eta]$ and its eigenfunctions are the Legendre polynomials. Therefore, accurate numerical solutions and simulations are obtained by projecting cell and nutrient density profiles onto the Legendre polynomial basis using Gauss-Legendre quadrature. Figure 1 shows the numerical simulation of evolution of a tumor clump initially in a homogeneous nutrient-rich environment. The tumor splits into two fronts which eventually reach the steady state moving at a constant speed. Analytically, the steady propagating front and its speed are determined by a shooting method. That is, to look for the steady states of Eqs. (4) and (5) in the inertial frame that moves with the same speed of the planar tumor. Assume the speed of the tumor front to be v , Eqs. (4) and (5) expressed in terms of the moving frame coordinates, $\zeta = x - vt$ and $\tau = t$, are

$$\frac{\partial n}{\partial \tau} = v \frac{\partial n}{\partial \zeta} + \frac{\partial^2 n}{\partial \zeta^2} + anA(u) - \gamma n - Mn(n - 1/2)(n - 1), \quad (6)$$

$$\frac{\partial u}{\partial \tau} = v \frac{\partial u}{\partial \zeta} + D_u \frac{\partial^2 u}{\partial \zeta^2} - nA(u). \quad (7)$$

The steady states and the propagating speed v are obtained by requiring $\partial n/\partial \tau = 0$ and $\partial u/\partial \tau = 0$ with the given bound-

ary condition and asymptotics. The asymptotic forms for n and u can be readily obtained by solving the steady state of the above equations linearized around the boundary values. That is, let $n = \delta n$ and $u = C_0 + \delta u$, and the linearized equations are

$$\frac{\partial}{\partial \zeta} \begin{pmatrix} \delta n \\ \partial \delta n / \partial \zeta \\ \delta u \\ \partial \delta u / \partial \zeta \end{pmatrix} = \begin{pmatrix} 0 & 1 & 0 & 0 \\ M/2 + \gamma - A(C_0) & -v & 0 & 0 \\ 0 & 0 & 0 & 1 \\ A(C_0)/D_u & 0 & 0 & -v/D_u \end{pmatrix} \times \begin{pmatrix} \delta n \\ \partial \delta n / \partial \zeta \\ \delta u \\ \partial \delta u / \partial \zeta \end{pmatrix}. \quad (8)$$

For large values of ζ , one readily obtains $n_{\text{asym}} = \delta n_1 e^{-h_1 \zeta}$ and $u_{\text{asym}} - C_0 = \delta u_1 e^{-h_1 \zeta} + \delta u_2 e^{-h_2 \zeta}$, where $h_1 = v/2 + \sqrt{v^2/4 + M/2 + \gamma - aA(C_0)}$ and $h_2 = v/D_u$, and $\delta n_1, \delta u_1, \delta u_2$ are components of corresponding eigenvectors. The shooting solutions of the tumor and nutrient densities (n_0, u_0) are plotted in Fig. 2 for various values of C_0 . It is shown that the cell density is not uniform across the tumor rim since the proliferation rate depends on the local nutrient density. In addition, the tumor density profile appears to be larger and thicker when in contact with a nutrient-richer environment as expected, since more nutrients are accessible to tumor cells away from the front surface. The propagating speed of the tumor also increases when in contact with a nutrient-richer environment, since the proliferation rate of cells increases with nutrient density. For the planar tumor, we obtain $v = 1.452$ and $v = 1.764$ for $C_0 = 6$ and $C_0 = 9$, respectively. It is worth noting that there exists a threshold value of C_0 below which the environment is too harsh and no nontrivial solution can be found. In addition to the shooting method, the steady moving front profile can be obtained alternatively by evolving Eqs. (6) and (7) with different speeds until the profile no longer changes and moves. With the steady planar tumor front and nutrient density profiles as the unperturbed states, the stability of perturbations in cell and nutrient densities is

examined to shed light on the mechanism behind the morphological instability of the tumor front.

B. Stability of planar solid tumor fronts

To investigate the morphological instability of planar solid tumors, small perturbations in tumor cell density n_1 and nutrient density u_1 are applied to the unperturbed steady state (u_0, n_0) in the moving frame such that $n(\zeta, y) = n_0(\zeta) + n_1(\zeta, y)$ and $u(\zeta, y) = u_0(\zeta) + u_1(\zeta, y)$. Note that perturbations only depend on ζ and y due to the rotational symmetry of the planar front. To examine the stability of the planar tumor front against perturbations of a different wave number k , the perturbations are assumed to have the following form:

$$\begin{pmatrix} n_1 \\ u_1 \end{pmatrix} = \begin{pmatrix} \bar{n}_{1k}(\zeta) \\ \bar{u}_{1k}(\zeta) \end{pmatrix} e^{\lambda_k t} e^{iky}, \quad (9)$$

where $\bar{n}_{1k}(\zeta)$ and $\bar{u}_{1k}(\zeta)$ are eigenfunctions which correspond to the largest growth rate of the perturbation λ_k . By substituting the ansatz into Eqs. (6) and (7) and retaining only linear terms of perturbations, we get

$$\frac{\partial n_1}{\partial \tau} = v \frac{\partial n_1}{\partial \zeta} - k^2 n_1 + \frac{\partial^2 n_1}{\partial \zeta^2} + \left. \frac{\partial F_1}{\partial n} \right|_{(n_0, u_0)} n_1 + \left. \frac{\partial F_1}{\partial u} \right|_{(n_0, u_0)} u_1, \quad (10)$$

$$\begin{aligned} \frac{\partial u_1}{\partial \tau} = v \frac{\partial u_1}{\partial \zeta} - D_u k^2 u_1 + D_u \frac{\partial^2 u_1}{\partial \zeta^2} + \left. \frac{\partial F_2}{\partial n} \right|_{(n_0, u_0)} n_1 \\ + \left. \frac{\partial F_2}{\partial u} \right|_{(n_0, u_0)} u_1, \end{aligned} \quad (11)$$

where $F_1(n, u) \equiv anA(u) - \gamma n - Mn(n - 1/2)(n - 1)$ and $F_2(n, u) \equiv -nA(u)$. Numerically, $\bar{n}_{1k}(\zeta)$, $\bar{u}_{1k}(\zeta)$, and λ_k are obtained by evolving the above equations while rescaling n_1 and u_1 constantly to a small number until shape-preserving solutions are reached. The growth rate λ_k is measured after the transient period by calculating $(\partial n_1 / \partial \tau) / n_1$ for nonvanishing n_1 . Figure 3 shows an example of eigenfunctions for which $k = 0.042$ and $\lambda_k = 0.0116$. The variation of tumor cells occurs in the region that is very close to the tumor surface, and the anticorrelation between n_1 and u_1 near the tumor surface reflects the fact that more tumor cells consume more nutrients. Furthermore, a dip in n_1 away from the tumor front is a direct result of insufficient nutrients due to more nutrients being consumed by tumor cells at the front surface.

For perturbations of different wave numbers, the stability of a planar tumor front is examined by evaluating the corresponding λ_k . For a fixed value of C_0 , short wavelength perturbations is shown to be suppressed while the stability of long wavelength perturbations depends on the value of C_0 ; see Fig. 4. The suppression of short wavelength perturbations is due to the tumor surface energy which reflects the nature of cell-cell adhesion, which will be discussed in detail later. However, for long wavelength perturbation, the instability is driven by the difference in the proliferation rate of cells at peaks and troughs along the wave. The difference in the proliferation rate comes from the difference in the contact nutrient density, which also results in the difference in the cell density at peaks and troughs. Once the difference is established, more cells at peaks consume more nutrients which leaves less nutri-

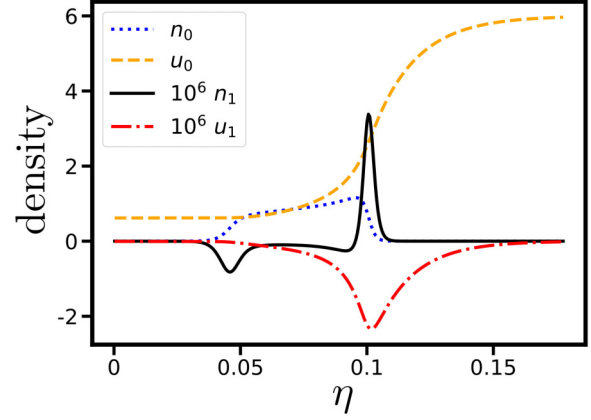


FIG. 3. Snapshot of the unperturbed steady states and the shape-preserving eigenfunctions of small perturbations. The blue dotted line and the yellow dashed line represent the unperturbed steady state of tumor cell density and nutrient density, respectively. The black solid line and the red dash-dotted line represent the shape-preserving eigenfunctions of n_1 and u_1 multiplied by 10^6 , respectively. The results are obtained with parameters $(C_0, a, \gamma, M, D_u, \bar{u}) = (6.0, 1, 0.4, 4.2, 10, 2)$ and $k = 0.042$. The growth rate of the perturbation is $\lambda_k = 0.0116$.

ents for cells at troughs, which further enhances the difference in the proliferation rate; hence, the instability occurs. The morphological instability of planar tumor fronts as discussed here, therefore, depends on the competition between the stabilizing surface tension and the destabilizing nutrient-regulated proliferation rate. However, since the proliferation rate of cells saturates in a nutrient-rich environment, the difference in the proliferation rate for cells at peaks and troughs decreases which makes the planar tumor surface stable. Figure 4 plots the dispersion relation for perturbations on planar tumors placed in environments with different nutrient densities at the boundary. For $C_0 = 6$, the nutrients are sufficient for tumor

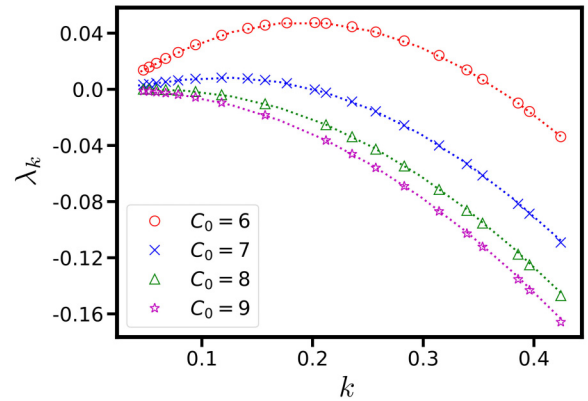


FIG. 4. Dispersion relation for various boundary nutrient densities ranging from $C_0 = 6$ to $C_0 = 9$. The symbols show the growth rate of the perturbation from the simulation results of Eqs. (6) and (7). The dotted lines show the linear analysis of Eqs. (10) and (11) for the boundary nutrient densities $C_0 = 6, 7, 8, 9$ from top to bottom, respectively. The results are obtained with parameters $(a, \gamma, M, D_u, \bar{u}) = (1, 0.4, 4.2, 10, 2)$.

to survive, but the nutrient density is relatively low so that the proliferation rate of cells is quite sensitive to the local nutrient density, which is in favor of the instability. As C_0 increases, the proliferation rate of cells shifts closer toward the saturated value, which makes the proliferation rate less sensitive to the nutrient density and the planar tumor front becomes relatively stable. The growth rate of the perturbation of a given wave number is also measured from direct numerical simulations of Eqs. (6) and (7) in two dimensions. Simulation results are in quantitatively good agreement with the linear stability analysis as shown in Fig. 4. Numerical simulations further show that, as the perturbation grows, the instability, in time, leads up to the breakup of tumor fronts and fragmented tumors. The fragmentation of solid tumors increases its contact surface to nutrients that boosts the overall growth of tumors, which is consistent with the previous results reported in Refs. [6,7,22,50].

It is worth noting that the instability is more pronounced as the surrounding nutrient density decreases, and the solid tumor eventually dies when the surrounding nutrient density is below a threshold. As solid tumors are placed in a harsher environment, the nutrient-dependent growth itself would empower solid tumors more easily with the capability of breaking up into small tumor clumps. Our results suggest that a nutrient-dependent growth rate could be the key factor that improves the odds for tumor survival by tumor fragmentations when the solid tumor is situated in a nutrient-deficient environment.

As discussed above, the morphological instability of tumor fronts also depends on its surface energy which is directly related to the cell-cell adhesion. Quantitatively, the surface energy of solid tumor fronts can be determined by examining the restoring force for perturbations of large wave numbers. In the limit of large wave numbers, the dispersion curves are well fitted by a quadratic relation, $\lambda_k = -\sigma k^2$, which implies a local growth mechanism of tumor cells at peaks and troughs [71]. And σ is proportional to the surface energy of the tumor front. The surface energy of planar tumor fronts is shown to depend on the surrounding nutrient density C_0 at infinity; see Fig. 5. This dependence arises from different steady tumor front profile which varies with C_0 . See Fig. 2 for examples. By assuming a constant cell-cell adhesion, the surface energy simply depends on the tumor density profile across the tumor rim. In Fig. 5, the surface energy is shown to be approximately proportional to the total number of cells per unit surface area defined as $n_{rim} = \int_{rim} n dx$, where the integration is performed across the tumor front. Therefore, tumors in a nutrient-richer environment form thicker rims and hence higher surface energies are expected, which also suppresses the morphological instability.

In addition to the surrounding nutrient density C_0 at infinity, we examine how the growth coefficient a affects the morphological instability. The growth coefficient a varies from different types of solid tumor cells, and a faster tumor velocity is usually associated with a larger growth coefficient. As discussed above, for a fixed growth coefficient a , three possible scenarios for tumor growth are found, namely, dying out of tumors at low C_0 , breakups of tumors at sufficient but low C_0 , and steady moving tumor fronts in the nutrient-rich environment. A phase diagram of tumor growth as a function

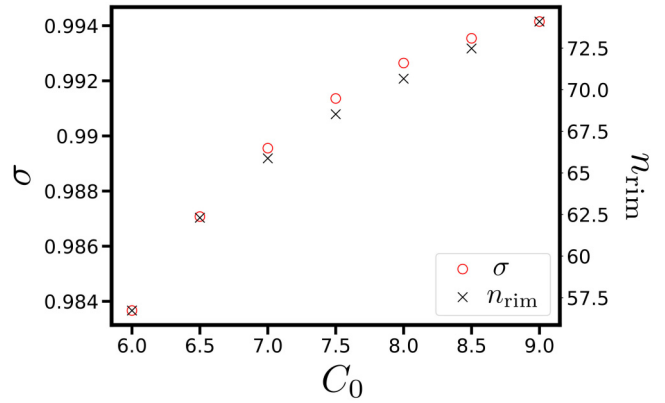


FIG. 5. σ and the total number of cells per unit surface area n_{rim} for various boundary nutrient densities. The results show that the surface energy is approximately proportional to the total number of cells per unit surface area. Results are obtained with parameters $(a, \gamma, M, D_u, \bar{u}) = (1, 0.4, 4.2, 10, 2)$.

of the growth coefficient a and the surrounding nutrient density C_0 is plotted in Fig. 6.

Interestingly, our results show that the morphological instability of tumor surfaces is suppressed when the growth coefficient a increases. However, for a given nutrient density, a larger growth coefficient would effectively enlarge the difference in proliferation rate between tumor cells at perturbing peaks and troughs, which should in principle enhance the instability but not suppress it. Previous studies report that the morphological instability is influenced by the front speed, but how the propagating speed affects the instability is inclusive [7,17,18,34]. To explicitly examine the relation between front speed and the instability, Fig. 7(a) plots the front speed for different growth coefficients a as well as different boundary nutrient densities C_0 . For a given C_0 , the instability is shown to be suppressed as the front speed increases, which is consistent with the observation that the instability is suppressed with increasing growth coefficient a . However, the onset speed of the instability, below which the tumors start to

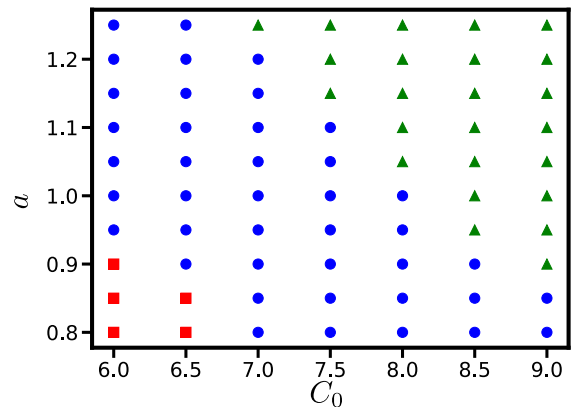


FIG. 6. Phase diagram for the avascular solid tumor growth. Red squares represent the phase of dying out of tumor cells. Blue circles and green triangles are breakups of tumors and steady moving tumor fronts, respectively. The phase diagram is obtained for parameters $(\gamma, M, D_u, \bar{u}) = (0.4, 4.2, 10, 2)$.

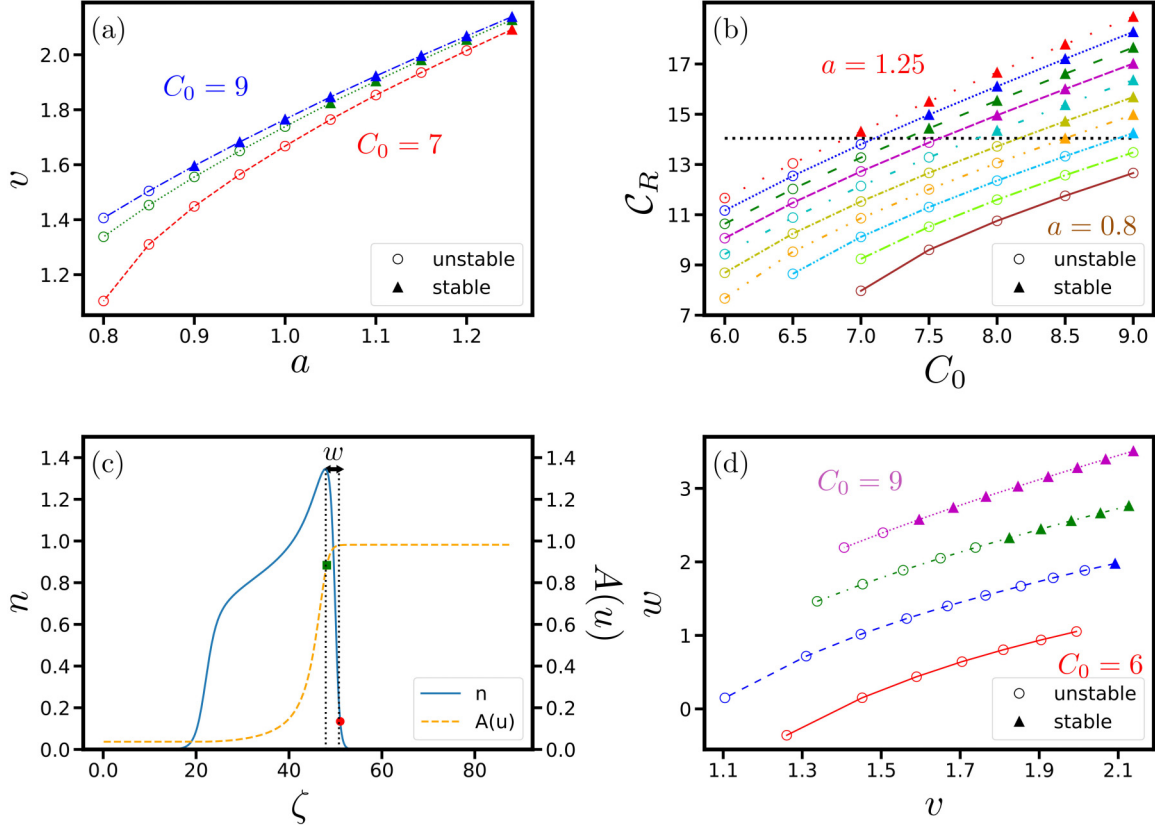


FIG. 7. (a) Front speed of different growth coefficients for different boundary nutrient density values. The boundary nutrient densities are $C_0 = 7, 8,$ and 9 for the red dashed line, green dotted line, and blue dash-dotted line, respectively. Empty circles represent the state breakups of tumors, and filled triangles represent the state of steady moving tumor fronts, and the same representation is used in panels (b) and (d). (b) Net flux of nutrient C_R of different boundary nutrient density values for different growth coefficients. Different colors and line styles represent different growth coefficients a . Taking $C_0 = 9$, for instance, the coefficients are $(0.8, 0.85, 0.9, 0.95, 1, 1.05, 1.1, 1.15, 1.2, 1.25)$ from bottom to top, respectively. The black dotted horizontal line shows the threshold of C_R above which systems prefer steady moving tumor fronts. (c) Illustration of the definition of nourished length w . The simulation is obtained with parameters $C_0 = 9$ and $a = 1$. The red circle is the position where front tumor density n reaches ten percent of its maximum value, and the green square is the position where the growth function $A(u)$ decreases to ninety percent of its maximum value. (d) Nourished length w of different front speeds for different boundary nutrient density values. The boundary nutrient values are $C_0 = 6, 7, 8,$ and 9 for the red solid line, blue dashed line, green dash-dotted line, and purple dotted line, respectively. The results of these four figures are obtained with parameters $(\gamma, M, D_u, \bar{u}) = (0.4, 4.2, 10, 2)$.

break up, clearly depends on the value of C_0 . To gain a more quantitative understanding of the morphological instability, the net flux of nutrients in and out of the planar tumor is calculated since this quantity indicates whether tumors find itself in a nutrient-rich environment or not. The net flux of nutrient, C_R , can be obtained by integrating Eq. (7) from the $\zeta = 0$ to $\zeta = \infty$ across a steady planar tumor profile. That is,

$$C_R = v \int_0^{\infty} \frac{\partial u}{\partial \zeta} d\zeta = v(C_0 - u_0) = \int_0^{\infty} nA(u)d\zeta, \quad (12)$$

where u_0 is the nutrient density deep in the necrosis region at $\zeta = 0$. The net flux of nutrient, C_R , also equals to the nutrients being consumed by tumor cells per unit area as evident in the last equality. The onset of the instability is shown to be well characterized by the proposed quantity C_R , see Fig. 7(b). There seems to exist a threshold of C_R above which tumor cells at the front surface are in contact with high nutrient density which diminishes the difference in the proliferation rate if perturbations are applied.

Since whether the tumor cells at the front surface can access sufficient nutrients is crucial for the morphological instability, a nourished length w , defined as the coordinate difference between the position where front tumor density n reaches ten percent of its maximum value and the position where the growth function $A(u)$ decreases to ninety percent of its maximum value, is employed to examine the instability. Figure 7(c) illustrates an example of defining the nourished length w , and how the nourished length w varies with the tumor front speed v and surrounding nutrient density C_0 is plotted in Fig. 7(d). For a given C_0 , the nourished length is shown to be positively correlated with the front speed since faster moving tumor fronts invade further into the nutrient-rich environment. Therefore, the instability is expected to be further diminished as the tumor front moves faster that is qualitatively consistent with previous results reported in Refs. [17,18].

It is clear that the nourished length depends on not only the tumor front speed but also on the types of nutrients such as oxygen, glucose, etc. Previous experimental results suggest

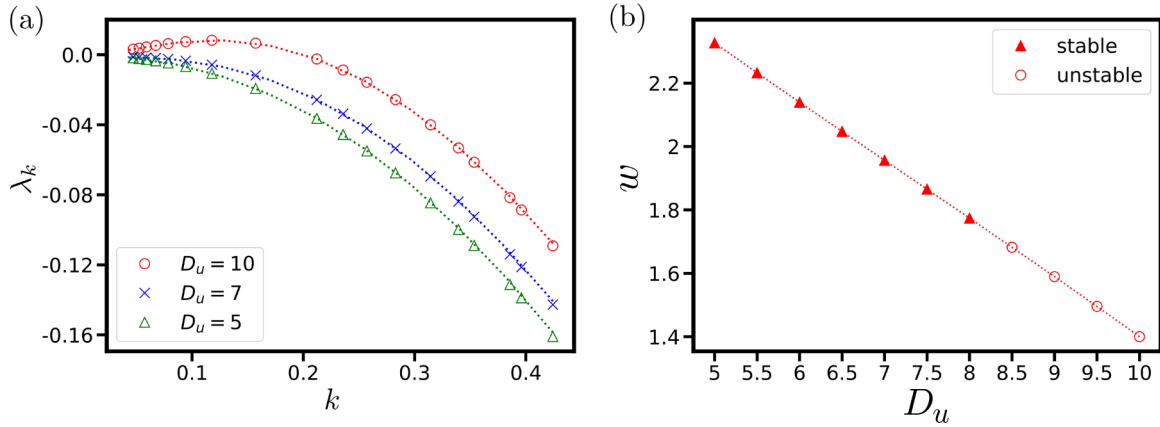


FIG. 8. (a) Dispersion relation for various diffusion coefficients ranging from $D_u = 5$ to $D_u = 10$. The symbols show the growth rate of the perturbation from the simulation results of Eqs. (6) and (7). The dotted lines show the linear analysis of Eqs. (10) and (11) for diffusion coefficients $D_u = 10, 7, 5$ from top to bottom, respectively. (b) Nourished length w of different diffusion coefficients. Empty circles are the state of breakups of tumors, and filled triangles represent the state of steady moving tumor fronts. Both results are obtained with parameters $(C_0, a, \gamma, M, \bar{u}) = (7, 1, 0.4, 4.2, 2)$.

that the nutrient diffusion coefficient is crucial to the morphological instability of the tumor [33,34]. For our model, the stability of planar tumor fronts in contact with nutrients with different diffusion coefficients is shown in Fig. 8(a). It shows that the morphological instability of tumor fronts can be induced more easily when tumors are placed in nutrients which are more diffusive. The results agree with the numerical investigation of human U87 brain tumor cells and Glioblastoma multiforme in which tumors are shown to be less invasive when nutrients are less diffusive [33,34]. This phenomenon can be understood from the perspective of the nutrient diffusion length. Since the diffusion length is proportional to $\sqrt{D_u}$, a less diffusive nutrient supply would have a rather sharply changing nutrient density profile near the tumor surface. Therefore, the tumor cells at the front surface are able to get closer to the nutrient-rich region when the tumor is in contact with a less diffusive nutrient supply; see Fig. 8(b). The nourished length increases as the diffusion coefficient of nutrients is reduced, which suppresses the morphological instability of tumor surfaces.

IV. SUMMARY AND DISCUSSION

In this paper, we investigate how the proliferation rate of tumor cells and the microenvironment affect the morphological instability of the avascular tumor growth. A set of reaction-diffusion equations for the tumor cell density and the nutrient density is proposed to describe the spatiotemporal growth of cells and distribution of nutrients which are main determinants for the surface instability. Based on experimental observations, the nutrient-dependent proliferation rate is assumed to be positively correlated to the local nutrient density when the nutrient density is low, and to saturate to a constant value when the nutrient density is high. It gives rise to three possible scenarios for the tumor growth, namely, dying out of tumors when it is subject to insufficient nutrients, breakups of tumors when it is subject to low but sufficient nutrients, and steady moving tumor fronts without breaking up when it is subject to high nutrients.

To better understand this phenomenon analytically, a linear stability analysis of perturbations applied to steady moving planar tumor fronts is employed. We find that, in the current model, the surface instability is driven by the difference in the proliferation rate of cells along the undulated surface, and is stabilized by the surface tension of tumor fronts. When the surrounding nutrient density is high, the difference in the proliferation rate of cells is minimal due to the saturating behavior of the proliferation rate at high nutrient density. Hence, perturbations decay and one observes steady moving planar tumor fronts. When the surrounding nutrient density is reduced, consumption of nutrients by tumor cells at the perturbing peaks on the surface would have a more pronounced influence on the local nutrient density at the perturbing troughs, which enlarges the difference in the proliferation rate, and hence the instability occurs. The instability eventually leads to breakups of tumor rims and fragmentations of tumors. By doing so, tumor cells gain more access to the nutrients, due to the increase in its overall surface area, to better its survival odds. The surface instability is shown to be stronger when the surrounding nutrient density is further reduced until the nutrient density is too low for tumors to survive. It appears that the nutrient-dependent proliferation nature alone could help tumors to develop a smart strategy of splitting up when facing a harsh environment.

In addition to the surrounding nutrient density, we investigate the relation between the tumor front speed and the surface instability. We find that the instability would be more suppressed when the tumor front moves faster, which is consistent with reported experiments. However, we show that the front speed alone is not a good indicator for the instability to occur. As discussed above, since the instability is closely related to the proliferation rate of tumor cells at the surface, the nutrients consumed by tumor cells per surface area or the proximity between tumor front surface and nutrient-rich region would be better indicators. By defining a nourished length w which represents the depth of tumor cells at the front surface into the nutrient-rich region, the instability is shown to be suppressed as w increases as expected. Furthermore, the effects of nutri-

ents with different diffusivity on the instability is discussed. Nutrients with different diffusivity result in different nutrient density distribution near the tumor surface, and the distribution is clearly crucial to the surface instability. We find that the instability is less pronounced as the nutrient diffusivity is reduced. It is because the nutrient density profile drops faster for nutrients with small diffusivity, and hence a larger nourished length.

In this study, the proposed model is used to investigate the morphological instability of planar tumor fronts due to the nutrient-dependent proliferation rate. It is of interest to extend the current discussion to explore the morphological instability for tumors with curved surfaces, that is,

tumor spheroids. Also, the formation of fragmented tumors in the later stage of avascular tumor growth can be studied numerically with the proposed model, which might be relevant to the beginning of aggressive neoplasia and tumor invasion [3,4,18].

ACKNOWLEDGMENTS

The authors gratefully acknowledge the support of the National Science and Technology Council, Taiwan (Grant No. MOST 111-2112-M-007-024), and the support from the National Center for Theoretical Sciences, Taiwan.

C.-H.Y. and Y.-C.L. contributed equally to this work.

-
- [1] L. M. Sander and T. S. Deisboeck, Growth patterns of microscopic brain tumors, *Phys. Rev. E* **66**, 051901 (2002).
- [2] T. S. Deisboeck, M. E. Berens, A. R. Kansal, S. Torquato, A. O. Stemmer-Rachamimov, and E. A. Chiocca, Pattern of self-organization in tumour systems: Complex growth dynamics in a novel brain tumour spheroid model, *Cell Proliferation* **34**, 115 (2001).
- [3] M. Basan, J.-F. Joanny, J. Prost, and T. Risler, Undulation Instability of Epithelial Tissues, *Phys. Rev. Lett.* **106**, 158101 (2011).
- [4] H. Kittler, P. Guitera, E. Riedl, M. Avramidis, L. Teban, M. Fiebiger, R. A. Weger, M. Dawid, and S. Menzies, Identification of clinically featureless incipient melanoma using sequential dermoscopy imaging, *Arch. Dermatol.* **142**, 1113 (2006).
- [5] T. Hoshino, M.-W. Liu, K.-A. Wu, H.-Y. Chen, T. Tsuruyama, and S. Komura, Pattern formation of skin cancers: Effects of cancer proliferation and hydrodynamic interactions, *Phys. Rev. E* **99**, 032416 (2019).
- [6] V. Cristini, H. B. Frieboes, R. Gatenby, S. Caserta, M. Ferrari, and J. Sinek, Morphologic instability and cancer invasion, *Clin. Cancer Res.* **11**, 6772 (2005).
- [7] H. B. Frieboes, X. Zheng, C.-H. Sun, B. Tromberg, R. Gatenby, and V. Cristini, An integrated computational/experimental model of tumor invasion, *Cancer Res.* **66**, 1597 (2006).
- [8] R. M. Enmon Jr., K. C. O'Connor, D. J. Lacks, D. K. Schwartz, and R. S. Dotson, Dynamics of spheroid self-assembly in liquid-overlay culture of du 145 human prostate cancer cells, *Biotechnol. Bioeng.* **72**, 579 (2001).
- [9] H. Byrne and P. Matthews, Asymmetric growth of models of avascular solid tumours: Exploiting symmetries, *Math. Med. Biol.* **19**, 1 (2002).
- [10] P. S. Steeg, Angiogenesis inhibitors: Motivators of metastasis? *Nat. Med.* **9**, 822 (2003).
- [11] H. Greenspan, Models for the growth of a solid tumor by diffusion, *Stud. Appl. Math.* **51**, 317 (1972).
- [12] H. Greenspan, On the growth and stability of cell cultures and solid tumors, *J. Theor. Biol.* **56**, 229 (1976).
- [13] J. S. Lowengrub, H. B. Frieboes, F. Jin, Y.-L. Chuang, X. Li, P. Macklin, S. M. Wise, and V. Cristini, Nonlinear modelling of cancer: Bridging the gap between cells and tumours, *Nonlinearity* **23**, R1 (2010).
- [14] S. M. Wise, J. S. Lowengrub, H. B. Frieboes, and V. Cristini, Three-dimensional multispecies nonlinear tumor growth I: Model and numerical method, *J. Theor. Biol.* **253**, 524 (2008).
- [15] V. Cristini, J. Lowengrub, and Q. Nie, Nonlinear simulation of tumor growth, *J. Math. Biol.* **46**, 191 (2003).
- [16] X. Zheng, S. M. Wise, and V. Cristini, Nonlinear simulation of tumor necrosis, neo-vascularization and tissue invasion via an adaptive finite-element/level-set method, *Bull. Math. Biol.* **67**, 211 (2005).
- [17] C. Chatelain, P. Ciarletta, and M. B. Amar, Morphological changes in early melanoma development: Influence of nutrients, growth inhibitors and cell-adhesion mechanisms, *J. Theor. Biol.* **290**, 46 (2011).
- [18] M. Ben Amar, C. Chatelain, and P. Ciarletta, Contour Instabilities in Early Tumor Growth Models, *Phys. Rev. Lett.* **106**, 148101 (2011).
- [19] T. Balois and M. B. Amar, Morphology of melanocytic lesions *in situ*, *Sci. Rep.* **4**, 3622 (2014).
- [20] M. Chaplain, Avascular growth, angiogenesis and vascular growth in solid tumours: The mathematical modelling of the stages of tumour development, *Math. Comput. Model.* **23**, 47 (1996).
- [21] T. Roose, S. J. Chapman, and P. K. Maini, Mathematical models of avascular tumor growth, *SIAM Rev.* **49**, 179 (2007).
- [22] P. Macklin and J. Lowengrub, Nonlinear simulation of the effect of microenvironment on tumor growth, *J. Theor. Biol.* **245**, 677 (2007).
- [23] C. Chatelain, T. Balois, P. Ciarletta, and M. B. Amar, Emergence of microstructural patterns in skin cancer: A phase separation analysis in a binary mixture, *New J. Phys.* **13**, 115013 (2011).
- [24] J. A. Sherratt and M. A. Nowak, Oncogenes, antioncogenes, and the immune response to cancer: a mathematical model, *Proc. R. Soc. London B* **248**, 261 (1992).
- [25] C. Märkl, G. Meral, C. Surulescu *et al.*, Mathematical analysis and numerical simulations for a system modeling acid-mediated tumor cell invasion, *Int. J. Anal.* **2013**, 878051 (2013).
- [26] A. M. Fouad, Dynamical stability analysis of tumor growth and invasion: A reaction-diffusion model, *Oncogen* **2**, 20 (2019).
- [27] T. Gallay and C. Mascia, Propagation fronts in a simplified model of tumor growth with degenerate cross-dependent self-diffusivity, *Nonlinear Anal. Real World Appl.* **63**, 103387 (2022).

- [28] A. R. A. Anderson, M. A. J. Chaplain, E. L. Newman, R. J. C. Steele, and A. M. Thompson, Mathematical modelling of tumour invasion and metastasis, *Comput. Math. Methods Med.* **2**, 129 (2000).
- [29] D. Trucu, P. Lin, M. A. Chaplain, and Y. Wang, A multiscale moving boundary model arising in cancer invasion, *Multiscale Model. Simul.* **11**, 309 (2013).
- [30] P. R. Nyarko and M. Anokye, Mathematical modeling and numerical simulation of a multiscale cancer invasion of host tissue, *AIMS Math.* **5**, 3111 (2020).
- [31] K. R. Swanson, E. C. Alvord, Jr., and J. Murray, A quantitative model for differential motility of gliomas in grey and white matter, *Cell Proliferation* **33**, 317 (2000).
- [32] K. R. Swanson, C. Bridge, J. Murray, and E. C. Alvord, Jr., Virtual and real brain tumors: using mathematical modeling to quantify glioma growth and invasion, *J. Neurol. Sci.* **216**, 1 (2003).
- [33] E. Khain and L. M. Sander, Dynamics and Pattern Formation in Invasive Tumor Growth, *Phys. Rev. Lett.* **96**, 188103 (2006).
- [34] M. Castro, C. Molina-París, and T. S. Deisboeck, Tumor growth instability and the onset of invasion, *Phys. Rev. E* **72**, 041907 (2005).
- [35] G. Lorenzo, M. A. Scott, K. Tew, T. J. R. Hughes, Y. J. Zhang, L. Liu, G. Vilanova, and H. Gomez, Tissue-scale, personalized modeling and simulation of prostate cancer growth, *Proc. Natl. Acad. Sci. USA* **113**, E7663 (2016).
- [36] R. M. Sutherland, J. A. McCredie, and W. R. Inch, Growth of multicell spheroids in tissue culture as a model of nodular carcinomas 2, *J. Natl. Cancer Inst.* **46**, 113 (1971).
- [37] A. Szabó and R. M. Merks, Cellular Potts modeling of tumor growth, tumor invasion, and tumor evolution, *Front. Oncol.* **3**, (2013).
- [38] F. Graner and J. A. Glazier, Simulation of Biological Cell Sorting using a Two-Dimensional Extended Potts Model, *Phys. Rev. Lett.* **69**, 2013 (1992).
- [39] R. M. Merks and J. A. Glazier, A cell-centered approach to developmental biology, *Physica A* **352**, 113 (2005).
- [40] J. Chen, J. G. Story, and R. G. Hulet, Evolution of atomic motion in an intense standing wave, *Phys. Rev. A* **47**, 2128 (1993).
- [41] S. Bekisz and L. Geris, Cancer modeling: From mechanistic to data-driven approaches, and from fundamental insights to clinical applications, *J. Comput. Sci.* **46**, 101198 (2020), 20 years of computational science.
- [42] Y. Jiang, J. Pjesivac-Grbovic, C. Cantrell, and J. P. Freyer, A multiscale model for avascular tumor growth, *Biophys. J.* **89**, 3884 (2005).
- [43] S. Turner and J. A. Sherratt, Intercellular adhesion and cancer invasion: A discrete simulation using the extended potts model, *J. Theor. Biol.* **216**, 85 (2002).
- [44] A. Agosti, C. Cattaneo, C. Givero, D. Ambrosi, and P. Ciarletta, A computational framework for the personalized clinical treatment of glioblastoma multiforme, *Z. Angew. Math. Mech.* **98**, 2307 (2018).
- [45] A. Agosti, P. F. Antonietti, P. Ciarletta, M. Grasselli, and M. Verani, A cahn-hilliard-type equation with application to tumor growth dynamics, *Math. Methods Appl. Sci.* **40**, 7598 (2017).
- [46] J. Falco, A. Agosti, I. G. Vetrano, A. Bizzi, F. Restelli, M. Broggi, M. Schiariti, F. DiMeco, P. Ferroli, P. Ciarletta, and F. Acerbi, *In silico* mathematical modelling for glioblastoma: A critical review and a patient-specific case, *J. Clin. Med.* **10**, 2169 (2021).
- [47] J. C. L. Alfonso, K. Talkenberger, M. Seifert, B. Klink, A. Hawkins-Daarud, K. R. Swanson, H. Hatzikirou, and A. Deutsch, The biology and mathematical modelling of glioma invasion: A review, *J. R. Soc. Interface.* **14**, 20170490 (2017).
- [48] M. Protopapa, A. Zygianni, G. S. Stamatakos, C. Antypas, C. Armpilia, N. K. Uzunoglu, and V. Kouloulis, Clinical implications of *in silico* mathematical modeling for glioblastoma: A critical review, *J. Neuro-Oncol.* **136**, 1 (2018).
- [49] H. B. Frieboes, F. Jin, Y.-L. Chuang, S. M. Wise, J. S. Lowengrub, and V. Cristini, Three-dimensional multispecies nonlinear tumor growth II: Tumor invasion and angiogenesis, *J. Theor. Biol.* **264**, 1254 (2010).
- [50] V. Cristini, X. Li, J. S. Lowengrub, and S. M. Wise, Nonlinear simulations of solid tumor growth using a mixture model: Invasion and branching, *J. Math. Biol.* **58**, 723 (2009).
- [51] A. Friedman and F. Reitich, Analysis of a mathematical model for the growth of tumors, *J. Math. Biol.* **38**, 262 (1999).
- [52] H. Byrne and M. Chaplain, Growth of nonnecrotic tumors in the presence and absence of inhibitors, *Math. Biosci.* **130**, 151 (1995).
- [53] J. J. Casciari, S. V. Sotirchos, and R. M. Sutherland, Variations in tumor cell growth rates and metabolism with oxygen concentration, glucose concentration, and extracellular ph, *J. Cell. Physiol.* **151**, 386 (1992).
- [54] J. P. Freyer and R. M. Sutherland, Regulation of growth saturation and development of necrosis in EMT6/Ro multicellular spheroids by the glucose and oxygen supply, *Cancer Res.* **46**, 3504 (1986).
- [55] C. K. N. Li, The glucose distribution in 9l rat brain multicell tumor spheroids and its effect on cell necrosis, *Cancer* **50**, 2066 (1982).
- [56] A. A. Wheeler, W. J. Boettinger, and G. B. McFadden, Phase-field model for isothermal phase transitions in binary alloys, *Phys. Rev. A* **45**, 7424 (1992).
- [57] S. G. Kim, W. T. Kim, and T. Suzuki, Phase-field model for binary alloys, *Phys. Rev. E* **60**, 7186 (1999).
- [58] J.-Y. Tinevez, U. Schulze, G. Salbreux, J. Roensch, J.-F. Joanny, and E. Paluch, Role of cortical tension in bleb growth, *Proc. Natl. Acad. Sci. USA* **106**, 18581 (2009).
- [59] L. Sewalt, K. Harley, P. van Heijster, and S. Balasuriya, Influences of allee effects in the spreading of malignant tumours, *J. Theor. Biol.* **394**, 77 (2016).
- [60] A. M. Kramer, B. Dennis, A. M. Liebhold, and J. M. Drake, The evidence for allee effects, *Popul. Ecol.* **51**, 341 (2009).
- [61] W. C. Allee, *Animal Aggregations: A Study in General Sociology* (1931).
- [62] P. A. Stephens, W. J. Sutherland, and R. P. Freckleton, What is the allee effect? *Oikos* **87**, 185 (1999).
- [63] Y. Hirakawa, T. Yoshihara, M. Kamiya, I. Mimura, D. Fujikura, T. Masuda, R. Kikuchi, I. Takahashi, Y. Urano, S. Tobita, and M. Nangaku, Quantitating intracellular oxygen tension in vivo by phosphorescence lifetime measurement, *Sci. Rep.* **5**, 17838 (2015).
- [64] M. T. Islam, S. Tang, C. Liverani, S. Saha, E. Tasciotti, and R. Righetti, Non-invasive imaging of Young's modulus

- and Poisson's ratio in cancers in vivo, *Sci. Rep.* **10**, 7266 (2020).
- [65] D. C. Stewart, A. Rubiano, K. Dyson, and C. S. Simmons, Mechanical characterization of human brain tumors from patients and comparison to potential surgical phantoms, *PLoS ONE* **12**, 1 (2017).
- [66] D. Chauvet, M. Imbault, L. Capelle, C. Demene, M. Mossad, C. Karachi, A.-L. Boch, J.-L. Gennisson, and M. Tanter, In vivo measurement of brain tumor elasticity using intraoperative shear wave elastography, *Ultraschall Med.* **37**, 584 (2016).
- [67] S. Miyamoto, K. Atsuyama, K. Ekino, and T. Shin, Estimating the diffusion coefficients of sugars using diffusion experiments in agar-gel and computer simulations, *Chem. Pharmaceut. Bull.* **66**, 632 (2018).
- [68] M. Martín-Landrove, Reaction-diffusion models for glioma tumor growth, [arXiv:1707.09409](https://arxiv.org/abs/1707.09409).
- [69] P. Gerlee and A. R. A. Anderson, Diffusion-limited tumour growth: Simulations and analysis, *Math. Biosci. Eng.* **7**, 385 (2010).
- [70] J. Grote, R. Süsskind, and P. Vaupel, Oxygen diffusivity in tumor tissue (ds-carcinosarcoma) under temperature conditions within the range of 20–40°C, *Pflügers Arch.* **372**, 37 (1977).
- [71] D. Srolovitz, On the stability of surfaces of stressed solids, *Acta Metall.* **37**, 621 (1989).